
This copy is for your personal, non-commercial use only.

If you wish to distribute this article to others, you can order high-quality copies for your colleagues, clients, or customers by [clicking here](#).

Permission to republish or repurpose articles or portions of articles can be obtained by following the guidelines [here](#).

The following resources related to this article are available online at www.sciencemag.org (this information is current as of July 8, 2011):

Updated information and services, including high-resolution figures, can be found in the online version of this article at:

<http://www.sciencemag.org/content/332/6037/1528.full.html>

Supporting Online Material can be found at:

<http://www.sciencemag.org/content/suppl/2011/06/22/332.6037.1528.DC1.html>

A list of selected additional articles on the Science Web sites **related to this article** can be found at:

<http://www.sciencemag.org/content/332/6037/1528.full.html#related>

This article **cites 54 articles**, 9 of which can be accessed free:

<http://www.sciencemag.org/content/332/6037/1528.full.html#ref-list-1>

This article has been **cited by 2** articles hosted by HighWire Press; see:

<http://www.sciencemag.org/content/332/6037/1528.full.html#related-urls>

This article appears in the following **subject collections**:

Planetary Science

http://www.sciencemag.org/cgi/collection/planet_sci

scale of thermal lattice QCD computations via hadronic observables. Furthermore, this gives a scale for temperatures that is compatible with the resonance gas model, as shown in Fig. 3. As we discussed in the introduction, this closes a circle of inferences that shows that phenomena obtained in heavy ion collisions are fully compatible with hadron phenomenology and provides a first check in bulk hot and dense matter for the standard model of particle physics.

Conclusions and outlook. We have performed a direct comparison between experimental data from high-energy heavy ion collisions on net-proton number distributions and lattice QCD calculations of net-baryon number susceptibilities. The agreement between experimental data, lattice calculations, and a hadron resonance gas model indicates that the system produced in heavy ion collisions attained thermalization during its evolution. The comparison further enables us to set the scale for nonperturbative, high-temperature lattice QCD by determining the critical temperature for the QCD phase transition to be 175^{+1}_{-7} MeV.

This work reveals the rich possibilities that exist for a comparative study between theory and experiment of QCD thermodynamics and phase structure. In particular, the current work can be extended to the search for a critical point. In a thermal system, the correlation length (ξ) diverges at the critical point. ξ is related to various moments of the distributions of conserved quantities, such as net-baryons, net-charge, and net-strangeness. Finite size and dynamical effects in heavy ion collisions put constraints on the values of ξ (34). The lattice calculations discussed here and several QCD-based models have shown that moments of net-baryon distributions are related to baryon number susceptibilities and that the ratio

of cumulants $m_2 = \kappa\sigma^2$, which is related to the ratio of fourth-order to second-order susceptibilities, shows a large deviation from unity near the critical point. Experimentally, $\kappa\sigma^2$ can be measured as a function of $\sqrt{s_{NN}}$ (or T and μ_B) in heavy ion collisions. A nonmonotonic variation of $\kappa\sigma^2$ as a function of $\sqrt{s_{NN}}$ would indicate that the system has evolved in the vicinity of the critical point and thus could be taken as evidence for the existence of a critical point in the QCD phase diagram.

References and Notes

1. F. Wilczek, *Phys. Today* **52N11**, 11 (1999).
2. F. Wilczek, *Phys. Today* **53N1**, 13 (2000).
3. G. Sterman *et al.*, *Rev. Mod. Phys.* **67**, 157 (1995).
4. M. Peardon, V. Crede, P. Eugenio, A. Ostrovidov, *AIP Conf. Proc.* **1257**, 19 (2010).
5. I. Arsene *et al.*, *Nucl. Phys. A* **757**, 1 (2005).
6. B. B. Back *et al.*, *Nucl. Phys. A* **757**, 28 (2005).
7. J. Adams *et al.*, *Nucl. Phys. A* **757**, 102 (2005).
8. K. Adcox *et al.*, *Nucl. Phys. A* **757**, 184 (2005).
9. B. I. Abelev *et al.*, *Phys. Rev. C* **79**, 034909 (2009).
10. S. Borsanyi *et al.*, *J. High Energy Phys.* **1009**, 073 (2009).
11. Y. Aoki, Z. Fodor, S. Katz, K. Szabo, *Phys. Lett. B* **643**, 46 (2006).
12. M. Cheng *et al.*, *Phys. Rev. D* **74**, 054507 (2006).
13. C. Schmidt, paper presented at Quark Confinement and the Hadron Spectrum IX, 30 August 30 to 3 September 2010, Madrid, Spain; available at <http://arxiv.org/abs/1012.2230v1>.
14. F. R. Brown, N. H. Christ, Y. F. Deng, M. S. Gao, T. J. Woch, *Phys. Rev. Lett.* **61**, 2058 (1988).
15. Y. Aoki, G. Endrodi, Z. Fodor, S. D. Katz, K. K. Szabó, *Nature* **443**, 675 (2006).
16. P. Braun-Munzinger, J. Wambach, *Rev. Mod. Phys.* **81**, 1031 (2009).
17. J. Cleymans, K. Redlich, *Phys. Rev. Lett.* **81**, 5284 (1998).
18. R. V. Gavai, S. Gupta, *Phys. Lett. B* **696**, 459 (2011).
19. M. M. Aggarwal *et al.*, *Phys. Rev. Lett.* **105**, 022302 (2010).
20. M. A. Stephanov, K. Rajagopal, E. V. Shuryak, *Phys. Rev. D* **60**, 114028 (1999).

21. R. D. Pisarski, F. Wilczek, *Phys. Rev. D* **20**, 338 (1984).
22. S. Gupta, *PoS LATTICE2010*, 007 (2010).
23. B. I. Abelev *et al.*, *Phys. Rev. C* **81**, 024911 (2010).
24. B. Mohanty, *Nucl. Phys. A* **830**, 899c (2009).
25. μ_B of bulk nuclear matter is quoted in the usual convention adopted in relativistic treatments because anti-baryon production also needs to be accounted for. An alternative (nonrelativistic) definition that takes nucleon number to be fixed would give much smaller chemical potential. However, this does not correspond to the physics of baryon number fluctuations that we examine.
26. R. V. Gavai, S. Gupta, *Phys. Rev. D* **68**, 034506 (2003).
27. M. Asakawa, U. Heinz, B. Muller, *Phys. Rev. Lett.* **85**, 2072 (2000).
28. S. Jeon, V. Koch, *Phys. Rev. Lett.* **85**, 2076 (2000).
29. Y. Hatta, M. A. Stephanov, *Phys. Rev. Lett.* **91**, 102003 (2003).
30. S. Gupta, *PoS CPOD2009*, 25 (2009).
31. The impact parameter is determined through a Glauber Monte Carlo procedure. The selected events correspond to the most central 0 to 5% and 0 to 10% events of the total hadronic cross section in Au+Au collisions for $\sqrt{s_{NN}} = 200, 62.4, \text{ and } 19.6$ GeV, respectively.
32. The change in the radius of convergence in going from $m_\pi/m_\rho = 0.33$ to 0.2 is likely to be between 10 and 15% (22). The corresponding effect on m_3 is about 2% or less at the two highest energies and less than 20% at an energy of 19.6 GeV.
33. F. Karsch, K. Redlich, *Phys. Lett. B* **695**, 136 (2011).
34. B. Berdnikov, K. Rajagopal, *Phys. Rev. D Part. Fields* **61**, 105017 (2000).
35. M. G. Alford, K. Rajagopal, F. Wilczek, *Phys. Lett. B* **422**, 247 (1998).

Acknowledgments: We thank Z. Fodor, R. V. Gavai, F. Karsch, D. Keane, V. Koch, B. Mueller, K. Rajagopal, K. Redlich, H. Satz, and M. Stephanov for enlightening discussions. We acknowledge the Indian Lattice Gauge Theory Initiative for computational support, the Department of Atomic Energy—Board of Research in Nuclear Sciences through the project sanction 2010/21/15-BRNS/2026, the U.S. Department of Energy under contract DE-AC03-76SF00098, and the Chinese Ministry of Education.

21 February 2011; accepted 4 May 2011
10.1126/science.1204621

The Oxygen Isotopic Composition of the Sun Inferred from Captured Solar Wind

K. D. McKeegan,^{1*} A. P. A. Kallio,¹ V. S. Heber,¹ G. Jarzabinski,¹ P. H. Mao,^{1,2} C. D. Coath,^{1,3} T. Kunihiro,^{1,4} R. C. Wiens,⁵ J. E. Nordholt,⁵ R. W. Moses Jr.,⁵ D. B. Reisenfeld,⁶ A. J. G. Jurewicz,⁷ D. S. Burnett⁸

All planetary materials sampled thus far vary in their relative abundance of the major isotope of oxygen, ^{16}O , such that it has not been possible to define a primordial solar system composition. We measured the oxygen isotopic composition of solar wind captured and returned to Earth by NASA's Genesis mission. Our results demonstrate that the Sun is highly enriched in ^{16}O relative to the Earth, Moon, Mars, and bulk meteorites. Because the solar photosphere preserves the average isotopic composition of the solar system for elements heavier than lithium, we conclude that essentially all rocky materials in the inner solar system were enriched in ^{17}O and ^{18}O , relative to ^{16}O , by ~7%, probably via non-mass-dependent chemistry before accretion of the first planetesimals.

The gravitational collapse of a molecular cloud fragment 4.57 billion years ago led to an accretion disc of gas and dust, the

solar nebula, from which the Sun and planets formed. This nebula was approximately homogeneous with respect to isotopic abundances,

which, given that isotope ratios from various stellar nucleosynthetic processes vary widely, points to efficient mixing either in interstellar space or in the solar nebula. Thus, the discovery (1) that high-temperature minerals in carbonaceous chondrite meteorites are enriched preferentially in ^{16}O compared to ^{17}O and ^{18}O relative to the abundances in terrestrial samples was considered evidence for the presence of exotic material that escaped thorough mixing and thereby

¹Department of Earth and Space Sciences, University of California—Los Angeles (UCLA), Los Angeles, CA 90095–1567, USA. ²Division of Physics, Math, and Astronomy, California Institute of Technology (Caltech), Pasadena, CA 91125, USA. ³School of Earth Sciences, University of Bristol, Bristol BS8 1RJ, UK. ⁴Institute for Study of the Earth's Interior, Okayama University, Misasa, Tottori 682-0193, Japan. ⁵Los Alamos National Laboratory, Los Alamos, NM 87545, USA. ⁶Department of Physics and Astronomy, University of Montana, Missoula, MT 59812, USA. ⁷Center for Meteorite Studies, Arizona State University, Tempe, AZ 85287, USA. ⁸Division of Geological and Planetary Science, Caltech, Pasadena, CA 91125, USA.

*To whom correspondence should be addressed. E-mail: mckeegan@ess.ucla.edu

retained a memory of its distinct nucleosynthetic history. Later findings of the widespread nature of very large oxygen isotopic heterogeneities among meteoritic materials (2, 3) and the lack of correlation of these oxygen isotopic compositions with those of presolar components [e.g., (4, 5)] led to various proposals that the oxygen isotopic anomalies were instead generated by complex isotope-selective chemistry within a homogeneous nebula (6–10).

The nature of the processes, conditions, and events giving rise to oxygen isotope anomalies can be constrained with knowledge of the average initial oxygen isotopic composition of the solar nebula, which by mass balance is equivalent to the solar composition. Although oxygen is the third most abundant element composing the Sun (and the largest constituent of rocky planets), the solar oxygen isotopic composition has remained essentially unknown. The usual approach of inferring solar abundances from measurements of primitive meteorites is inadequate because of the aforementioned heterogeneities, and recent attempts to determine the Sun's oxygen isotopic composition from molecular absorption lines in the solar atmosphere are potentially prone to large systematic errors (11). To directly measure solar material, NASA flew the Genesis Discovery Mission to capture samples of the solar wind (SW) and return them to Earth for laboratory analysis (12).

Genesis orbited the Earth-Sun Lagrange point, L1, exposing collectors to the SW outside the Earth's magnetosphere between November 2001 and April 2004. In September 2004, the payload was returned to Earth; unfortunately, the parachute deployment mechanism failed and the sample return capsule struck Earth's surface at terminal velocity, shattering most of the target materials. In addition to passive collectors, Genesis included the Concentrator, a parabolic electrostatic mirror that reflected SW ions, focusing them onto backward-facing targets (13). Fortunately, these targets were suspended on a high-transparency wire mesh and survived the crash largely intact, suffering only some surface contamination. We selected an unbroken single-crystal SiC target (Fig. 1) for depth-profiling analysis by MegaSIMS, a hybrid secondary ion microscope–accelerator mass spectrometer (14) designed specifically to tackle the unique analytical challenges posed by the Genesis samples: dilute concentrations, limited sample material, and close proximity of surface contamination to the implanted SW ions. Here we report measurements of the oxygen isotopic composition of captured SW that demonstrate that the Earth and meteorites are grossly isotopically anomalous.

Isotopic measurement of captured solar wind. After inserting the sample into the analysis chamber of MegaSIMS (vacuum $<2 \times 10^{-11}$ Torr), we used reflected-light imaging to select areas that were free from defects or particles larger than a few micrometers. Even these apparently pristine areas were contaminated with oxygen adsorbed on the sample surface that ex-

ceeded the concentration of SW oxygen by orders of magnitude. We therefore cleaned the sample surface in situ by sputtering with a low-energy Cs beam rastered over $300 \mu\text{m}$ by $300 \mu\text{m}$ centered on the targeted area (Fig. 1) [supporting online material (SOM)]. Although the sputter cleaning removed the top ~ 20 nm of the sample, because of the low impact energy used (5 keV) only minimal amounts of surficial terrestrial oxygen were mixed into the implanted SW (14). After surface cleaning, we switched the MegaSIMS to analytical mode (20-keV impact energy, 20-nA Cs^+ rastered over $\sim 130 \mu\text{m}$ by $130 \mu\text{m}$) and used ion microscope imaging to briefly inspect the analytical area to ensure that it was free of contaminant dust particles larger than a few hundred nanometers. We employed frequent instrument baking and other measures to reduce levels of instrumental background to $<2\%$ of the SW fluence integrated over the top ~ 100 nm of the sample (SOM).

The MegaSIMS accelerated negative secondary ions to 10 keV, then passed them through an “isotope recombinator” mass filter (14) such that only masses 16 to 18 atomic mass units (amu) were injected into the tandem accelerator with its high-energy terminal held at +1.2 MV. Collisions with Ar gas stripped electrons from the incoming beam, destroying interfering molecular ions, including hydrides (14). We determined the in-depth distributions of implanted SW oxygen ions by simultaneous detection of the three O^{2+} isotope beams by ion counting (Fig. 2). To calibrate instrumental background, we continued sputtering through the implanted SW layer (peak

concentration depth ~ 80 nm) until a steady-state count rate was reached (typically at depths >300 nm). We corrected measured ion count rates for this background, for detector deadtime and duty cycle, and for mass-dependent isotopic fractionation in the MegaSIMS, which we determined by analysis of terrestrial standard materials under similar analytical conditions (SOM).

In principle, integration of the total counts in a depth profile yields the isotope ratios for the implanted SW. However, because of removal of the contaminated target surface, the integral cannot be taken over the entire SW profile. The implantation profiles (peak depth and width) are slightly different for each isotope as they depend on ion energy, and hence isotopic mass (15); accordingly, we fit a normal distribution to each isotope depth profile and summed the counts over the range from -1σ to 6σ relative to its peak depth. For a given depth profile, Poisson statistics limit the isotope ratio precision; analyses of oxygen-rich materials (terrestrial and meteoritic minerals) demonstrate accuracy of MegaSIMS to a level of $\sim 1\%$ (per mil).

The main purpose of the Concentrator was to increase both the effective fluence and implantation depth (16) of SW oxygen (and nitrogen) isotopes on the target collectors (13). The concentration factor is azimuthally symmetric, depending only on radial distance from the central axis of the Concentrator (17). However, because it must focus ions of different energies and different charge and mass, the Concentrator ion optics also impart a mass-dependent fractionation, which is a function of radial position on the

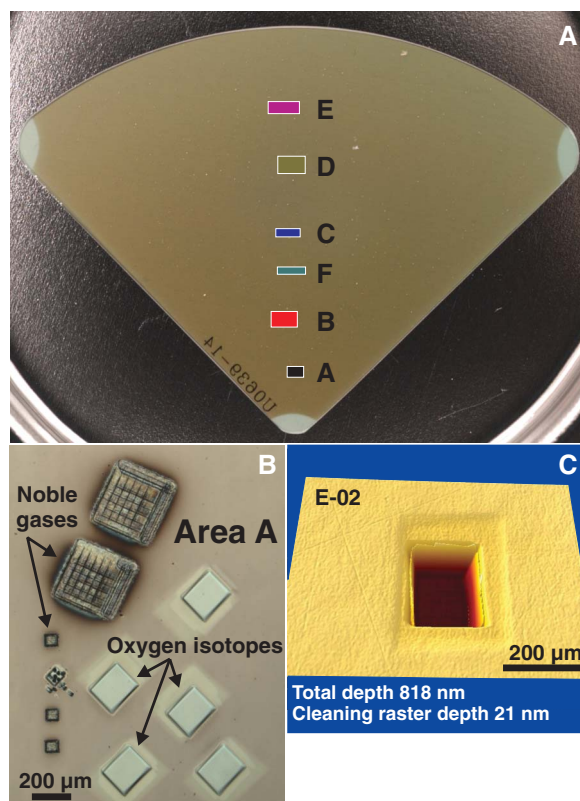


Fig. 1. (A) Photograph of Genesis SiC target 60001 (54) showing approximate areas analyzed along a radial traverse from inner region (area A) to periphery (area E) of the Concentrator. (B) Reflected-light micrograph of area A showing craters sputtered by Cs-beam rastering in MegaSIMS, along with two sets of pits made by laser ablation for noble gas analysis (17). The smaller pits were made to obtain $^{22}\text{Ne}/^{20}\text{Ne}$ data for correcting the mass-dependent fractionation induced at each radial position by the Concentrator ion optical system. (C) Rendering of surface topography made by an optical interferometer used to calibrate sputter rate. The effect of surface cleaning is visible as a shallow crater encompassing the area sampled by the deeper sputtered crater.

target. To assess the extent of concentration- and mass-dependent fractionation factors, we measured 40 depth profiles from 6 different areas in a traverse across the SiC sample (#60001) from 5.4 to 25.3 mm from the center (Fig. 1 and fig. S2). Neon isotopic compositions and fluence were later measured with high spatial resolution along the same radial traverse (17). The Ne isotope ratios of SW collected during the same period were previously determined in the bulk, passive SW collector, thereby permitting a direct measurement of the mass-dependent fractionation induced by the Concentrator as a function of target radius (17). We applied the Concentrator mass fractionation curve determined from $^{22}\text{Ne}/^{20}\text{Ne}$ to correct the $^{18}\text{O}/^{16}\text{O}$ and $^{17}\text{O}/^{16}\text{O}$ at each radial position (17) (SOM) (fig. S6).

From the interior (area “A”) to the exterior of the sample (area E, fig. S2), the implanted SW oxygen concentration decreases by a factor ~ 5 (fig. S3), consistent with the Ne traverse data (17). Of 40 depth profiles measured, 38 have integrated oxygen isotopic compositions that plot below the terrestrial mass fractionation line (TF), i.e., they are enriched in ^{16}O (SOM, table S1). Isotopic compositions from within the same area on the sample are reproducible, although the profiles from areas near the periphery of the target (areas D and E) show appreciable scatter because of poor counting statistics (fig. S5). The two profiles not enriched in ^{16}O come from area D and plot on the terrestrial mass fractionation line. The average compositions for each of the six areas analyzed (18) show clear evidence of mass-dependent fractionation, as expected on the basis of their radial positions on the Concentrator target (Fig. 3A). All analyses are consistent with an ^{16}O -rich composition for the captured SW with a mean $\Delta^{17}\text{O} = -28.4 \pm 1.8\text{‰}$ (Fig. 3C).

Correction of the measured $^{18}\text{O}/^{16}\text{O}$ and $^{17}\text{O}/^{16}\text{O}$ for Concentrator-induced mass-dependent fractionation as a function of radial position (17) (SOM) results in a convergence of all the data on a single composition within measurement uncertainties (Fig. 3B). Taking the average of the four areas measured within the interior 16 mm of the target (A, B, F, C), for which the concentration factors are highest ($>20\times$), we find that the SW collected by the Genesis spacecraft at L1 has a composition of $\delta^{18}\text{O} = -102.3 \pm 3.3\text{‰}$, $\delta^{17}\text{O} = -80.8 \pm 5.0\text{‰}$, where the uncertainty estimates are 1 standard deviation. In addition to being ^{16}O -enriched relative to terrestrial values, this composition is significantly to the left of the ^{16}O -mixing line defined by calcium-aluminum-rich inclusions (CAIs) of chondritic meteorites (19).

Inferring solar values from the solar wind.

In principle, the isotopic composition of SW oxygen collected at L1 could be equivalent to the photospheric value, but this is unlikely. First, spacecraft instruments (20, 21) and measurements on Genesis samples (22) detect enrichments of light isotopes in the low-speed relative to the fast SW, demonstrating that mass-dependent fractionation occurs in the acceleration of SW.

Both the sign (favoring light isotopes) and the magnitude—several percent for He (21, 22) and $<1\text{‰/amu}$ for heavier elements (22, 23)—are in approximate agreement with a model based on inefficient Coulomb drag (24). For a He/H ratio of 0.045 measured in the bulk SW on Genesis (25), this model predicts that the SW oxygen isotopic composition should be $\sim 26\text{‰/amu}$ lighter than the photosphere. Second, the existence of a SW-photosphere isotopic fractionation of this direction and magnitude is supported by the lack of meteoritic or planetary components with oxygen isotopic compositions plotting to the left of the CAI mixing line at the ^{16}O -enriched end (19, 26). Although many CAIs show mass-dependent fractionation favoring the heavy isotopes for non-refractory elements (e.g., Mg, Si), they rarely show mass fractionation effects in oxygen exceeding a few permil per amu. Those exceptions (i.e., the so-called FUN inclusions) have $\delta^{18}\text{O}$ values to the right of the CAI mixing line by tens of permil and are typically slightly less ^{16}O -enriched (i.e., less negative $\Delta^{17}\text{O}$) than our results for the SW (27).

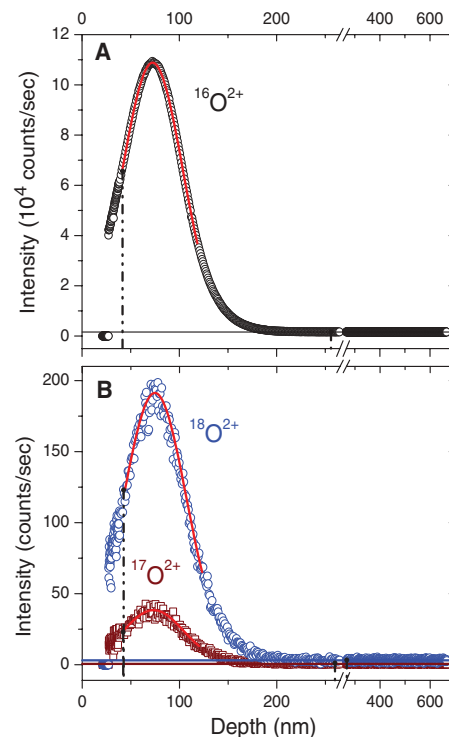


Fig. 2. In-depth distribution of implanted SW oxygen. Shown are measured ion intensity as a function of sputter depth for (A) $^{16}\text{O}^{2+}$ and (B) $^{17}\text{O}^{2+}$ and $^{18}\text{O}^{2+}$ in spot 4 of area A of the Genesis Concentrator SiC target 60001 and a normal distribution (red lines) fit to the peak of each profile. The top ~ 20 nm was removed by low-energy sputter cleaning; the first few measurement cycles have 0 counts because during this time the ion image was inspected for dust particles in the analytical area. Integration limits for each peak are indicated by vertical dashed lines (the small isotope specific differences are irresolvable at this scale). Note scale break at 265 nm. Background levels are indicated by horizontal lines.

These observations make it unlikely that the oxygen isotopic composition of CAIs resulted from mass-dependent fractionation from a solar composition equivalent to that measured for SW from L1. Given the consistent indications of fractionation from data in SW regimes, the model predictions, and expectations based on meteorite

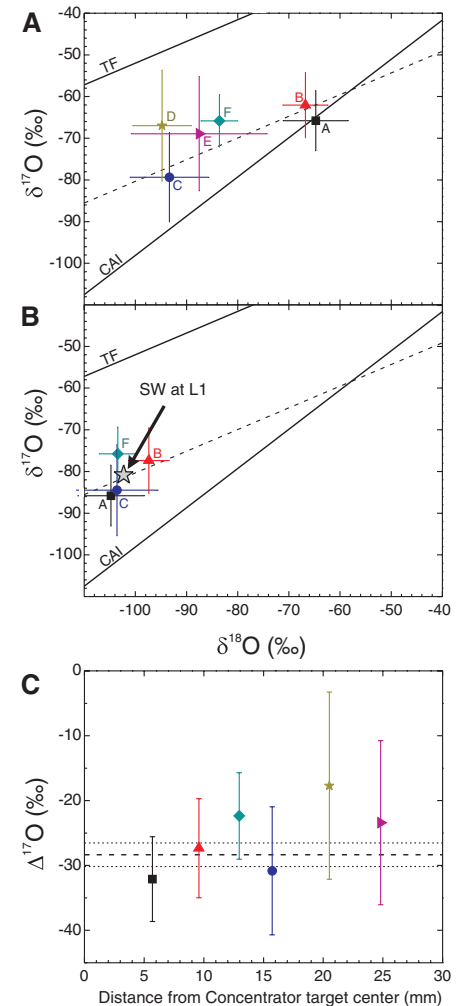


Fig. 3. (A) Mean oxygen isotopic compositions of SW from each group of depth profiles across a radial traverse of the Genesis Concentrator target. Shown are $\delta^{17}\text{O}$ and $\delta^{18}\text{O}$ corrected for instrumental mass fractionation in the MegaSIMS and normalized to standard mean ocean water (SMOW):

$$\delta^{18}\text{O} = \left(\frac{(^{18}\text{O}/^{16}\text{O})_{\text{sample}}}{(^{18}\text{O}/^{16}\text{O})_{\text{SMOW}}} - 1 \right) \times 1000, \text{ and similarly}$$

for $\delta^{17}\text{O}$. Shown for reference are the terrestrial mass-dependent fractionation line (TF) and the CAI mixing line (19). (B) SW oxygen isotope data from areas A, B, F, and C corrected for mass-dependent fractionation induced by the Concentrator (SOM). (C) The deviation from the terrestrial mass-dependent fractionation line expressed as $\Delta^{17}\text{O} = \delta^{17}\text{O} - (0.52 \times \delta^{18}\text{O})$ plotted as a function of radial position on the target. In (A) and (B), $\Delta^{17}\text{O}$ is the vertical displacement in $\delta^{17}\text{O}$ from a measured point to the TF line.

studies, we thus take as the most plausible composition of the Sun the intersection of the CAI mixing line with a mass-dependent fractionation line passing through the SW L1 point, which yields $\delta^{18}\text{O} = -58.5\%$, $\delta^{17}\text{O} = -59.1\%$ (Fig. 4). The total fractionation from SW to the Sun implied is $\sim 22\%$ /amu, in accordance with the model predictions.

The ^{16}O -enriched SW composition measured in the Genesis sample is in broad agreement with a component found from oxygen isotope measurements in the surface layers of some lunar metal grains (28) and of metal in a carbonaceous chondrite that shows evidence for SW exposure early in solar system history (29), although in both cases the data show a large degree of mass-dependent fractionation from the L1 SW value. Other analyses (30) of oxygen isotopes in a lunar regolith sample that indicate a ^{16}O -depleted composition ($\Delta^{17}\text{O} > 0$) probably reflect other extralunar sources, such as water brought by impacting interplanetary dust or cometary ices (31). Our measured SW composition is in marked contrast to the strongly ^{17}O - and ^{18}O -enriched values inferred from observations of rovibrational bands of CO in the solar atmosphere (32); we attribute this discrepancy to systematic uncertainties in the thermal profile models that underlie the abundance calculations (11). Our solar values of $^{16}\text{O}/^{18}\text{O} = 530$ and $^{16}\text{O}/^{17}\text{O} = 2798$ also disagree with other marginally ^{18}O -enriched values determined spectroscopically (33), although the data overlap within 2σ uncertainties.

The composition of the photosphere is thought to be representative of the convecting envelope of the Sun, representing $\sim 2.5\%$ of its

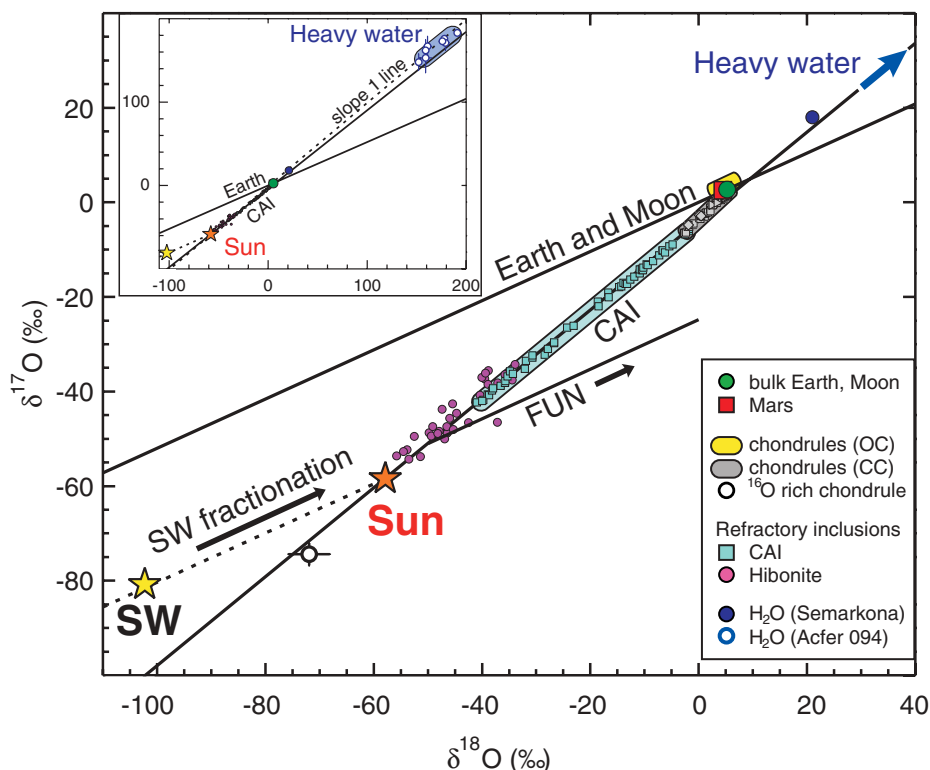
mass, perhaps modified slightly by gravitational settling of heavier elements [see (11)]. Although not directly determined, such settling could potentially lead to a small mass-dependent fractionation favoring retention of heavy isotopes deeper in the Sun, i.e., the same sense of fractionation as that caused by inefficient Coulomb drag in the SW (34). Other changes to the original isotopic composition of heavy elements in the photosphere are unlikely given that there is no mixing of nuclear processed matter into the convective zone (11). Fractionation mechanisms hypothesized as potentially operating in the solar atmosphere, e.g., mass-independent effects induced during dissociation of CO molecules in a cool layer of the chromosphere (35), are unlikely to lead to quantitative changes of the photospheric (or SW) oxygen isotopic abundances given the high temperatures (>3000 K) involved and rapidity of isotope exchange back-reactions and reservoir mixing in this dynamic environment. Thus, the large oxygen isotopic differences observed between the Sun and meteoritic or terrestrial samples are not caused by changes in solar matter, but instead reflect processes acting to induce mass-independent shifts in the oxygen isotopic compositions of planetary materials.

Implications for the solar nebula. The only known materials with oxygen isotopic compositions close to those of the Sun are the CAIs and other refractory phases of chondritic meteorites (Fig. 4), interplanetary dust (36), and at least one comet (37). CAIs are thought to be the earliest solar system condensates, and most crystallized with spallogenic beryllium and lithium, probably from proton bombardment in the magnetically

active environment near the still-accreting proto-Sun (38, 39). That their oxygen isotopes are dominated by a solar, rather than planetary, component reinforces their status as xenoliths (2, 40, 41) in the asteroid belt. However, most CAIs, including ultrarefractory hibonite grains (Fig. 4), are not quite as ^{16}O -enriched as the Sun, implying some mixing with isotopically heavier oxygen from other solar system reservoirs.

Our results suggest that essentially all planetary objects in the inner solar system (<5 AU) have oxygen isotopic compositions distinct from the average of the solar nebula from which they formed, having been enriched by $\sim 70\%$ in both $^{18}\text{O}/^{16}\text{O}$ and $^{17}\text{O}/^{16}\text{O}$ by one or more non-mass-dependent fractionation processes before accretion. Considering that oxygen is by far the most abundant element in the terrestrial planets, this points to efficient, planetary-scale processes that, if based on molecular speciation, must involve the dominant O-bearing molecules in the solar nebula: CO, H_2O , and/or silicate dust (SiO, MgO, FeO, and others in combination). A leading hypothesis, which predicted our results (6), invokes isotope-selective self-shielding during ultraviolet (UV) photolysis of CO. Because of their relatively low abundances, the C^{17}O and C^{18}O isotopomers continue to be dissociated after all the photons capable of dissociating C^{16}O have been absorbed; the liberated ^{17}O and ^{18}O atoms are then rapidly sequestered into H_2O ice and eventually are incorporated into oxide and silicate grains (7, 10). The places and times where this results in a slope 1 fractionation trajectory on the oxygen three-isotope plot (i.e., in pure enrichment or depletion of ^{16}O) are constrained by gas column

Fig. 4. Oxygen three-isotope plot showing representative compositions of major primary components of solar system matter, the solar wind (SW), and our preferred value for the Sun. All data fall predominantly on a single mixing line characterized by excesses (lower left) or depletions (upper right) of ^{16}O relative to all samples of the Earth and Moon. Plotted are the most ^{16}O -enriched solar system samples: an unusual chondrule (47); individual platy hibonite grains (55), which are ultrarefractory oxides from carbonaceous chondrites (CC); water inferred to have oxidized metal to magnetite (56) in ordinary chondrites (OC); very ^{16}O -depleted water from the CC Acfer 094 (3), and whole CAIs from CC (19); and chondrules from CC and OC (19), bulk Earth (mantle), and Mars (SNC meteorites). The mass-dependent fractionation trajectory of primary minerals in FUN inclusions and the pure ^{16}O (slope 1.0) line (57) are also shown.



density and UV flux. If isotopic self-shielding is the mechanism, the distribution of isotopically heavy water ice and its interaction with the rock reservoir (42, 43) are critical, but presently poorly understood, problems.

Measurements of low-density anhydrous interplanetary dust particles (IDPs), which if derived from comets (as hypothesized) should not have exchanged oxygen isotopes with ices, do not support a dominantly ^{16}O -enriched dust reservoir as input into the solar nebula (44); however, the cometary origin of these IDPs is not firmly established, and many of the materials of the Jupiter family Comet Wild 2 sampled by the Stardust Mission originated in the inner solar system (37). Models that place CO gas and H_2O ice oxygen isotope fractionation in the cold molecular cloud preceding formation of the solar nebula [e.g., (10, 45)] usually assume that average primordial dust is relatively ^{16}O -rich, although this is not strictly required. That such a component has not been found in any appreciable abundance in meteorites or IDPs has led to an alternative interpretation: formation of planetary materials by mixing relatively $^{17,18}\text{O}$ -enriched ($\Delta^{17} \approx 0$) dust with (^{16}O -rich) solar gas at much greater than average solar nebula proportions of dust to gas (27). This mixing scenario relegates isotopic self-shielding to a minor effect and has the benefit of alleviating some uncomfortably tight chronological constraints on oxygen isotope processing. By contrast, the most ^{16}O -depleted solar system material found in meteorites (inset, Fig. 4) is thought to have been produced via direct oxidation by ^{16}O -depleted water ice (3), in line with expectations based on the isotopic-abundance-driven self-shielding mechanism. Additionally, astronomical observations of oxygen isotopic abundances in CO gas in accretion disks surrounding young stellar objects (46) have yielded evidence for non-mass-dependent fractionation consistent with the self-shielding UV photolysis model.

One chondrule has been found that is even more ^{16}O -enriched (47) than the solar value measured here; the significance of this is not clear. In a self-shielding model, it is possible that the chondrule acquired its oxygen through interaction with a CO-rich gas that had already been depleted of heavy isotopes of oxygen via UV-photolysis of the rare isotopologs. This would require transport or sequestering of the $^{17,18}\text{O}$ out of the region in which this chondrule or its precursors formed. In the mixing model (27), the chondrule would have formed in a strongly dust-depleted region of the solar nebula.

Alternative hypotheses to isotope-selective photochemical self-shielding are based on laboratory experiments (48) and observations (49) of gas-phase (9) or surface (8) chemistry wherein non-mass-dependent isotopic effects are manifestations of molecular symmetry-induced degeneracy effects on isotope reaction rates. So-called non-RRKM effects may also play a role during growth of silicate condensates via surface reac-

tions (8, 50); however, definitive experimental evidence for such effects on oxygen isotope abundances is currently lacking.

Analyses of $^{15}\text{N}/^{14}\text{N}$ in the same Genesis sample measured here demonstrate that planetary nitrogen is highly depleted in the light isotope ^{14}N relative to solar values to an extent not compatible with normal thermodynamically driven mass-dependent fractionation (51), possibly also pointing to a dominant role of photochemistry in setting volatile element isotope patterns in the solar accretion disk.

References and Notes

- R. N. Clayton, L. Grossman, T. K. Mayeda, *Science* **182**, 485 (1973).
- K. D. McKeegan, L. A. Leshin, S. S. Russell, G. J. MacPherson, *Science* **280**, 414 (1998).
- N. Sakamoto *et al.*, *Science* **317**, 231 (2007).
- A. J. Fahey, J. N. Goswami, K. D. McKeegan, E. K. Zinner, *Astrophys. J.* **323**, L91 (1987).
- L. R. Nittler *et al.*, *Astrophys. J.* **682**, 1450 (2008).
- R. N. Clayton, *Nature* **415**, 860 (2002).
- J. R. Lyons, E. D. Young, *Nature* **435**, 317 (2005).
- R. A. Marcus, *J. Chem. Phys.* **121**, 8201 (2004).
- M. H. Thieme, *Science* **283**, 341 (1999).
- H. Yurimoto, K. Kuramoto, *Science* **305**, 1763 (2004).
- M. Asplund, N. Grevesse, A. J. Sauval, P. Scott, *Annu. Rev. Astron. Astrophys.* **47**, 481 (2009).
- D. S. Burnett *et al.*, *Space Sci. Rev.* **105**, 509 (2003).
- R. C. Wiens *et al.*, *Space Sci. Rev.* **105**, 601 (2003).
- P. H. Mao, D. S. Burnett, C. D. Coath, G. Jarzabinski, K. D. McKeegan, *Appl. Surf. Sci.* **255**, 1461 (2008).
- At any one time, the SW is a constant-velocity plasma; thus, isotopes vary in kinetic energy. The difference in implantation depth in the Concentrator target is ~ 1.5 nm per mass unit at the peak of the profile.
- The -6.5 kV potential of the interior of the Concentrator resulted in higher implantation energies in the range of 46 to 100 keV for oxygen's dominant charge states of +6 and +7 and incident velocities of 300 to 800 km/s. Typical incident angles at the target are 10° to 55° from normal for the main portion of the target, resulting in depth profiles with peaks near 80 nm.
- V. S. Heber *et al.*, *Meteorit. Planet. Sci.* **46**, 493 (2011).
- One profile from area B was removed from the average because it is known to be partially contaminated by a dust particle (SOM).
- R. N. Clayton, *Annu. Rev. Earth Planet. Sci.* **21**, 115 (1993).
- P. Bodmer, P. Bochsler, *Astron. Astrophys.* **337**, 921 (1998).
- G. Gloeckler, J. Geiss, in *Light Elements and Their Evolution*, L. DaSilva, M. Spite, J. R. DeMedeiros, Eds. (AIU Symposium, 2000), vol. 198, pp. 224–233.
- V. S. Heber, R. C. Wiens, P. Bochsler, R. Wieler, D. S. Burnett, *Lunar Planet. Sci.* **XL**, 2503 (2009).
- R. Kallenbach *et al.*, *Space Sci. Rev.* **85**, 357 (1998).
- R. Bodmer, P. Bochsler, *J. Geophys. Res. Space Phys.* **105**, 47 (2000).
- The hydrogen fluence is derived from the ion monitor on the Genesis spacecraft and the helium fluence is measured in the Genesis target by (52).
- K. D. McKeegan, L. A. Leshin, in *Stable Isotope Geochemistry*, J. W. Valley, D. R. Cole, Eds. (Mineralogical Society of America, Washington, DC, 2001), vol. 43, pp. 279–318.
- A. N. Krot *et al.*, *Astrophys. J.* **713**, 1159 (2010).
- K. Hashizume, M. Chaussidon, *Nature* **434**, 619 (2005).
- K. Fujimoto, S. Itoh, S. Ebata, H. Yurimoto, *Geochem. J.* **43**, e11 (2009).
- T. R. Ireland, P. Holden, M. D. Norman, J. Clarke, *Nature* **440**, 776 (2006).
- K. Hashizume, M. Chaussidon, *Geochim. Cosmochim. Acta* **73**, 3038 (2009).
- T. R. Ayres, C. Plymate, C. U. Keller, *Astrophys. J. Suppl. Ser.* **165**, 618 (2006).
- P. C. Scott, M. Asplund, N. Grevesse, A. J. Sauval, *Astron. Astrophys.* **456**, 675 (2006).
- If the Sun's composition lies on the CAI-mixing line, as we hypothesize, then gravitational settling would result in the photosphere being slightly displaced to the left by $\sim 3\%$ /amu, depending on the model (53).
- A. Yamada, S. Nanbu, Y. Kasai, M. Ozima, *Lunar Planet. Sci.* **XLII**, 1707 (2011).
- K. D. McKeegan, *Science* **237**, 1468 (1987).
- K. D. McKeegan *et al.*, *Science* **314**, 1724 (2006).
- K. D. McKeegan, M. Chaussidon, F. Robert, *Science* **289**, 1334 (2000).
- M. Chaussidon, F. Robert, K. D. McKeegan, *Geochim. Cosmochim. Acta* **70**, 224 (2006).
- T. J. Fagan, K. D. McKeegan, A. N. Krot, K. Keil, *Meteorit. Planet. Sci.* **36**, 223 (2001).
- Y. Guan, K. D. McKeegan, G. J. MacPherson, *Earth Planet. Sci. Lett.* **181**, 271 (2000).
- J. R. Lyons *et al.*, *Geochim. Cosmochim. Acta* **73**, 4998 (2009).
- E. D. Young, *Earth Planet. Sci. Lett.* **262**, 468 (2007).
- J. Aléon, C. Engrand, L. A. Leshin, K. D. McKeegan, *Geochim. Cosmochim. Acta* **73**, 4558 (2009).
- G. Dominguez, *Astrophys. J.* **713**, L59 (2010).
- R. L. Smith, K. M. Pontoppidan, E. D. Young, M. R. Morris, E. F. van Dishoeck, *Astrophys. J.* **701**, 163 (2009).
- K. Kobayashi, H. Imai, H. Yurimoto, *Geochem. J.* **37**, 663 (2003).
- M. H. Thieme, J. E. Heidenreich III, *Science* **219**, 1073 (1983).
- M. H. Thieme, T. L. Jackson, C. A. M. Breninkmeijer, *Geophys. Res. Lett.* **22**, 255 (1995).
- A. Ali, J. A. Nuth, *Astron. Astrophys.* **467**, 919 (2007).
- B. Marty, M. Chaussidon, R. C. Wiens, A. J. G. Jurewicz, D. S. Burnett, *Science* **332**, 1533 (2011).
- V. S. Heber *et al.*, *Geochim. Cosmochim. Acta* **73**, 7414 (2009).
- S. Turcotte, R. F. Wimmer-Schweingruber, *J. of Geophys. Res.* **107**, 1442 (2002).
- A. J. G. Jurewicz *et al.*, *Space Sci. Rev.* **105**, 535 (2003).
- M. C. Liu *et al.*, *Geochim. Cosmochim. Acta* **73**, 5051 (2009).
- B. G. Choi, K. D. McKeegan, A. N. Krot, J. T. Wasson, *Nature* **392**, 577 (1998).
- E. D. Young, S. S. Russell, *Science* **282**, 452 (1998).

Acknowledgments: We gratefully acknowledge financial support from the NASA programs Discovery, SRLIDAP/LARS, and Cosmochemistry. The ultimate success of the Genesis Discovery Mission would not have been possible without major engineering contributions from the Los Alamos National Laboratory (Concentrator), Jet Propulsion Laboratory (payload, mission operations, management), Lockheed Martin Aerospace (spacecraft and re-entry capsule), and the Johnson Space Center (payload integration and curation). The MegaSIMS laboratory received financial support from UCLA and NASA as well as important technical support from the National Electrostatics Corporation, Kore Technology Ltd, CAMECA, and R. Plue. We benefited from expert advice from J. Huneke, C. Evans Jr., M. Suter, H. Sinal, K. Grabowski, S. Smith, and P. Williams. We appreciate collaborations with the accelerator team at Orsay, led by J. Duprat and G. Slodzian. The sample investigated here was well cared for by J. Allton, E. Stansbery, and their Johnson Space Center team. We are grateful for help and advice from A. Davis, D. Papanastassiou, N. Vogel, R. Wieler, D. Woolum, the reviewers of this manuscript, and the entire Genesis Science Team.

Supporting Online Material

www.sciencemag.org/cgi/content/full/332/6037/1528/DC1
Materials and Methods
Figs. S1 to S6
Tables S1 and S2
References and Notes

21 February 2011; accepted 10 May 2011
10.1126/science.1204636